ELSEVIER

Catalysis Today 38 (1997) 97–105

CATALYSIS TODAY

# Effect of unsteady-state catalyst surface on the SCR-process

E.S. Borisova, A.S. Noskov*, L.N. Bobrova

*Boreskov Institute of Catalysis, Prospekt Akademika Lavrentieva 5, 630090 Novosibirsk, Russia*

**Abstract**

The kinetic model of nitrogen oxides reduction by ammonia on vanadium-containing catalysts considering the dynamic character ammonia surface interaction with $NO_x$ and oxygen served as a base of mathematical model of unsteady-state processes in the fixed catalyst bed. The theoretical analysis of the model helped to study the catalytic reactor behavior, when the stoichiometric ratio of reagents $NO_x/NH_3$ is disturbed. A distribution of adsorbed ammonia along the catalyst bed was studied as a function of time between the reverses of gas flow passing through the catalyst bed. The model allowed to describe qualitatively the high degrees (up to 99%) of gas conversion of $NO_x$ obtained using a large scale plant.

## 1. Introduction

In the 70s Prof. Matros et al. suggested a method of catalytic process performance under a periodic reverse of flow in a catalyst bed thus using the fixed bed thermal inertia. At present this method is widely used for gas purification [1–4]. Another way to increase the catalytic process efficiency using the unsteady-state catalyst surface has not yet been fully developed.

As the composition of the gas phase or its temperature vary, the state of the catalyst changes, and the latter comes to a new steady state [5]. Depending on the type of catalytic reaction, catalyst used and reaction conditions this transition may long from several seconds to dozen minutes [5]. During the transition the catalyst activity may differ essentially from the steady state one.

The dynamic catalyst properties may expose a great effect on the processes going in the reactor. For the selective catalytic reduction of $NO_x$ by ammonia it has been shown that NO conversion measured under the steady-state conditions can be lower than that observed during the unsteady-state tests [6]. As the phase composition varies, reaction rate changes rather slowly. In the transient experiments of Schneider et al. [7], when $NH_3$ emits from the reagent flow, or NO and $O_2$ containing mixture is exposed to the $NH_3$-loaded catalyst, $N_2$ and $H_2O$ concentrations decrease, and the signal from NO in the product gas increases for about 7 min.

Ammonia adsorbs on the catalyst surface producing various species [8]. Strongly adsorbed NO was also detected during the SCR occurrence. The rate of SCR process is faster than the net rate of ammonia desorption [9]. Ammonia accumulation on the catalyst surface can thus have a smoothing effect at the distortion of ratio $NH_3/NO$.

Such features of SCR reaction allow to suggest new method of reaction performance. In the paper of Agar and Ruppel [10] regimes, appearing in an isothermal catalytic reactor under the oscillations of reagent concentrations, are considered provided for ammonia

*Corresponding author. Tel.: (7-383) 235-7678/0178; Fax: (7-3830 235-7678; e-mail: alex@reverse.nsk.su


*PII* S0920-5861(97)00043-6

adsorption and its surface interaction with nitrogen oxides. In [11] steady- and unsteady-state regimes were studied experimentally in the bed of a zeolite catalyst. It has been found that it is possible to improve the process efficiency in the dynamic regime.

The authors of Refs. [12,13] have designed a way to purify low-temperature exhaust gases from $NO_x$. The method comprises a periodic reverse of the gas flow filtered through the catalyst bed at a simultaneous ammonia introduction into the catalyst bed center. This method was up-scaled and brought into practice in 1989. Its efficiency proved to be rather high.

The present paper concerns a theoretical study of the processes occurring in the SCR reactors and uses a mathematical model considering the unsteady state of the catalyst, system heterogeneity, solid phase thermal inertia, and convective heat (mass) transfer in the gas phase. Regimes, appearing in the reactor at the change of reaction mixture composition at reactor inlet and/or at periodic reverses of the gas flows in the catalyst beds, were the object of the present study.

## 2. Process mathematical model

In the course on NO reduction by ammonia the basic reactions are the following:

$$4NO + 4NH_3 + O_2 = 4N_2 + 6H_2O$$

$$4NH_3 + 3O_2 = 2N_2 + 6H_2O.$$

The kinetic models for the mathematical description SCR process have been constructed assuming the simplest mechanism concerning the catalyst surface dynamics [10,12,14]:

$$NH_3 + [\,] \Leftrightarrow [NH_3] + \Delta H_{ads} \quad \text{(I)}$$

$$[NH_3] + NO + 1/4O_2 \rightarrow N_2 + 3/2H_2O + [\,] + \Delta H_{red} \quad \text{(II)}$$

$$[NH_3] + 3/4O_2 \rightarrow 1/2N_2 + 3/2H_2O + [\,] + \Delta H_{oxid}. \quad \text{(III)}$$

This mechanism makes possible to take into account the adsorption capacity of vanadium catalyst surface. For typical SCR catalysts this capacity is about 10 ammonia volumes per catalyst volume.

The change of adsorbed ammonia concentration ($\theta$) is described by equation:

$$a\frac{d\theta}{dt} = W_1 - W_2 - W_3 \quad (1)$$

where

$$W_1 = k_1^+ \hat{C}_1(1-\theta) - k_1^- \theta$$

– the rate of reversible $NH_3$ adsorption; (2)

$$W_2 = k_2 \hat{C}_2 \theta$$

– rate of adsorbed ammonia interaction with NO; (3)

$W_3 = k_3\theta$ – rate of adsorbed $NH_3$ oxidation. (4)

$a$ – is the adsorption capacity of the catalyst surface ($cm^3NH_3/cat\ cm^3$), $a$=5–10.

The numerical values of the constants and $\Delta H$ for the reaction occurring in various reductions and oxidations have been estimated from the literature [1,2] and by test [15,16]:

$$k_1^+ = 0.74 \times 10^{12}\exp(-23000/RT);$$

$$k_1^- = 0.87 \times 10^{7}\exp(-26800/RT);$$

$$k_2 = 0.35 \times 10^{6}\exp(-8400/RT);$$

$$k_3 = 0.31 \times 10^{13}\exp(-31600/RT);$$

$$\Delta H_{ads} = 34 \times 10^3\ \text{kcal/mol};$$

$$\Delta H_{red} = 63.8 \times 10^3\ \text{kcal/mol};$$

$$\Delta H_{oxid} = 41.5 \times 10^3\ \text{kcal/mol},$$

where $R = 1.987\ \text{cal mol}^{-1}\ \text{K}^{-1}$ is the universal gas constant and $\Delta H$ the enthalpy of reaction.

One can find the SCR rate at steady state, assuming Eq. (1) equal to zero and solving it with respect to $\theta$. Introducing the found $\theta^*$ into Eqs. (3) and (4) one can find the rate of $NO_x$ reduction and ammonia oxidation at steady state.

The dynamic regimes occurring in the fixed bed reactor over the unsteady-state catalyst surface are described by the following set of equations:

Gas phase:

$$\varepsilon \cdot U\frac{\partial C_i}{\partial l} = \beta(\hat{C}_i - C_i), \quad i = 1,2 \quad (5)$$

$$\varepsilon \cdot U\frac{\partial T}{\partial l} = \alpha(T_S - T) \quad (6)$$

$$\beta(\hat{C}_i - C_i) = -W_i, \quad i = 1,2 \tag{7}$$

where specific mass and heat transfer coefficients $\beta$ and $\alpha$ are defined as follows:

$$\beta = \beta_0 \cdot S$$

$$\alpha = \alpha_0 \cdot S$$

Solid phase:

$$a\frac{d\theta}{dt} = W_1 - W_2 - W_3 \tag{8}$$

$$\gamma \cdot \frac{\partial T_s}{\partial t} = \lambda\frac{\partial^2 T_s}{\partial l^2} - \alpha(T_s - T) + \sum_{i=1}^{3}\Delta T_{ad,i} \cdot W_i, \tag{9}$$

where $\gamma = (1-\varepsilon)C_c/C_p$ is the dimensionless relative heat capacity of catalyst bed; $\lambda = \lambda_{eff}/C_p$ the specific coefficient of thermal conductivity of catalyst bed frame; and $\Delta T_{ad,i} = Q_i/C_p$ the adiabatic heating of $i$th reaction.

Boundary conditions

$$l = 0: \; C_i = C_i^{in}; \; T = T^{in}; \tag{10}$$

$$\lambda\frac{\partial T_s}{\partial l} = 0 \tag{11}$$

$$l = L: \; \lambda\frac{\partial T_s}{\partial l} = 0 \tag{12}$$

$$t = 0: \; T_s = T_s^0(l); \; \theta = \theta^0(l) \tag{13}$$

The model is written, as no diffusion restriction inside the catalyst grains is assumed. Other assumptions are typical for the two-phase model in the adiabatic reactor. Similar mathematical models have been investigated in Refs. [1] and [17]. To calculate via model (2)–(14) we used a complex numerical–analytical method often applied for the problems of this type [18]. Non-linear Eq. (9) was solved with spline approximations using non-direct difference scheme of the first order in time, non linear term $\sum \Delta T_{ad,i} W_i$ was taken over the previous time pixel. Eq. (6) has analytical solutions over each net length. Iteration process is used to correct the solutions of (6) and (9). To approximate the first derivatives in Eq. (5) (derivatives of a spatial variable) and (8) (derivative of time) the Euler scheme is applied with a second-order accuracy correction. A uniform net with a constant pixel is built for spatial variable $l$ (or for dimensionless variable $\xi \in [0,1]$, appearing when set (5)–(13) is rearranged to the dimensionless form). Time pixel can be variable and is chosen depending on the problem individuality.

## 3. Calculations results and their discussion

Studying equation set (2)–(13) we have considered the SCR reactor dynamics, when the composition of reaction mixture at the catalyst bed inlet varies as well as under periodic reverses of gas flow in the catalyst bed.

### 3.1. *Influence of inlet concentration oscillations on the SCR process efficiency*

Fig. 1 shows the concentrations of $NO_x$ and ammonia calculated using the unsteady and steady (the right part of Eq. (1) is equal to zero) kinetic models for the case of periodic (20 min) oscillation of the inlet $NO_x$ concentration from 0.4 vol% to zero. For a half cycle $NO_x$ concentration exceeds that of ammonia, SCR process occurring under reductant deficit. In the next cycle half a large excess of ammonia is fed. The average concentration of nitrogen oxides and ammonia in a cycle is 0.2 vol% (see Fig. 1A). In the first-half cycle a higher ammonia concentration is observed in

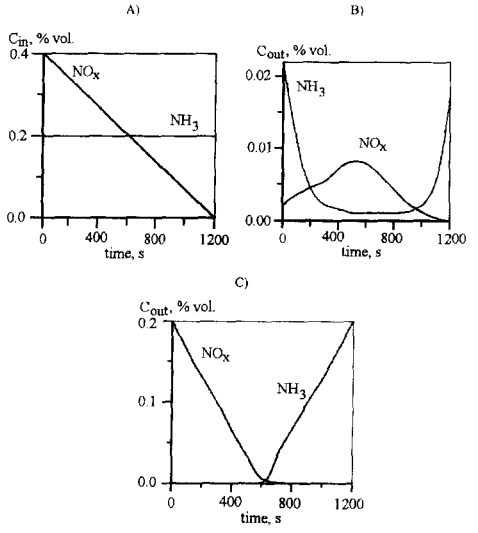


Fig. 1. Nitrogen oxides and ammonia concentration at the inlet (A) and outlet (B, C) of the bed. B – calculation via nonstationary model, C – calculation via stationary model. Continuous flow reactor. $T^{in} = 260°C$; $\tau_c = 0,4$ s.

the outlet flow notwithstanding its deficit. The reason is the desorption of some ammonia amounts accumulated in the previous half-cycle. The adsorbed ammonia comes into reaction, when the $NO_x$ content in the gas flow is high. As the adsorbed ammonia is consumed, the degree of gas purification from $NO_x$ decreases as well as ammonia slip. In the middle of the cycle, the situation changes as the excess ammonia appears in the gas phase at the catalyst bed inlet. Depending on the catalyst adsorption capacity ammonia content starts to increase at the outlet, while that of $NO_x$ starts to decrease. The concentration of nitrogen oxides at the bed outlet does not exceed 0.008 vol%, that of ammonia – 0.02 vol%. The SCR process simulation by the steady-state kinetic model shows that the output $NO_x$ and $NH_3$ concentrations change with the input ones (Fig. 1C). In the first half-cycle all excess nitrogen oxides (maximum 0.2 vol%) appear at the outlet. In the second half-cycle the same occurs with ammonia. Therefore, catalyst capacity toward ammonia adsorption helps the process efficiency at the accidental oscillations of the reagent concentrations.

### 3.2. *Effect of periodic gas flow reverse in the catalyst bed on the SCR process efficiency*

Fig. 2 shows schematic diagrams for a possible SCR performance under the reverse conditions. The catalyst bed is placed between two beds of packed heat accumulating material serving for heat recover prior to the start-up catalyst and inert beds are heated by a heater up to the temperature required for reaction start, 230–250°C. Then exhaust gases containing nitrogen oxides are mixed with ammonia and fed into the reactor. The inert zone gas is heated to the reaction temperature, and conversion occurs over the catalyst bed. After every 5–60 min the direction of the filtered gas flow is reversed.

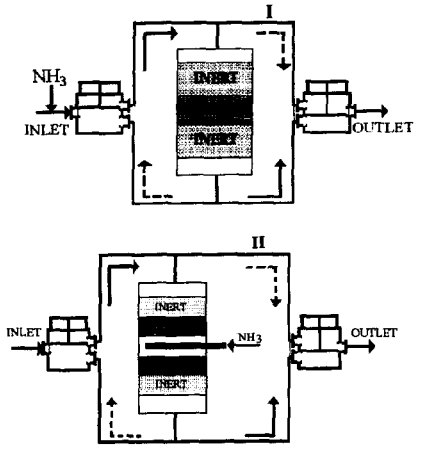


Fig. 2. Schematic diagram of the SCR process with a periodic flow reverse in the catalyst bed.

After several reverses an operation regime installs, when the temperature in the fixed bed center can be far higher than that in both end parts. By the second diagram ammonia is fed into the flow after the first part of the catalyst bed. In general terms, both temperature and concentration profiles along the catalyst bed depend on the parameters of the heat and mass transfer and reaction kinetics. Purification operation occurs by means of changing the time between the flow reverses, half-cycle duration.

Let us now consider how the characteristics of process, such as the distribution of adsorbed ammonia along the catalyst bed, the maximum value of temperature during the half-cycle period, the average content of ammonia accumulated on the catalyst surface during the half-cycle period and the conversion of $NO_x$ and $NH_3$ vary depending on the half-cycle time.

We are going to discuss the numerical results obtained only for diagram II, because they seem to be more representative and of great interest for practice. The comparison are also made with the results calculated using steady-state kinetic model.

Fig. 3 shows the ammonia distribution along the catalyst bed. In Fig. 3A, one can see that during the half-cycle ammonia coverage in the first part of the catalyst bed decreases due to the interaction with nitrogen oxides. After ammonia introduction its accumulation in the second part of the catalyst bed occurs. The same tendency takes place at the stoichiometric ammonia deficit ($NH_3$/NO ratio is equal to 0.85), see (Fig. 3B). By the steady-state kinetic model no reaction proceeds in the first part of the catalyst bed (Fig. 3C). Such a different manner of ammonia distribution along the catalyst bed imposes the differences in the process regimes calculated according to model (2)–(14) using the steady- and unsteady-state kinetic models.

According to the steady-state kinetic model, the maximum temperature in the catalyst bed is somewhat lower (by 5–10°C) than that of the unsteady-state

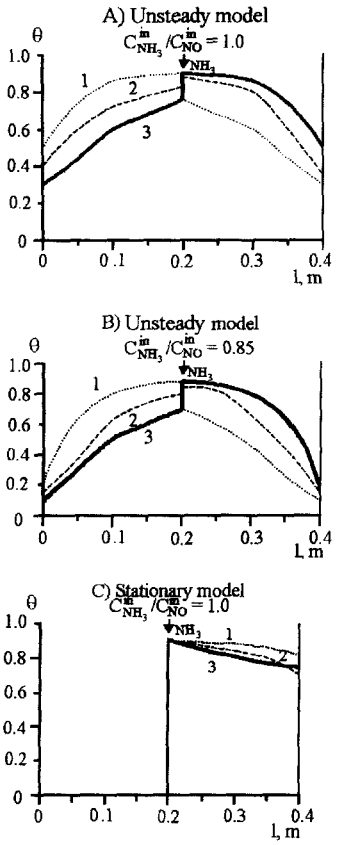


Fig. 3. Ammonia coverage profyles on the catalyst during one semi-cycle of reverse-reactor operation (diagram II).

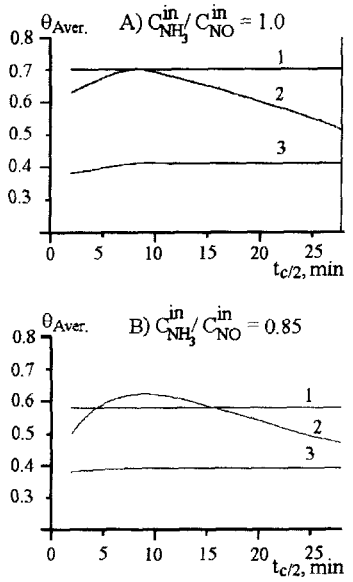


Fig. 4. Average ammonia store on the catalyst versus semi-cycle duration. 1 – continuous flow reactor; 2 – nonstationary model, reverse-reactor; 3 – stationary model, reverse-reactor.

catalyst. So, it is necessary to reduce time between reverses to obtain the same maximum temperature.

Other conditions being the same, the SCR process efficiency at flow reverses to a large extent depends on the frequency of the latter. Let us consider for diagram II, how the content of ammonia accumulated on the catalyst surface (Fig. 4), maximum temperature and conversion of $NO_x$ and $NH_3$ depend on the half-cycle time. Obviously, unsteady-state model provides an extreme dependence of ammonia accumulation between the reverses (Fig. 4, curve 2). At first, time period increase causes the growth average value of $\theta$ due to the decrease of the average heat accumulated in the bed (curve 2, Fig. 4). The curve passes through the maximum, and the amount of ammonia accumulated can exceed that calculated form the continuous flow reactor (curve 1, Fig. 4). As $t_{c/2}$ increases further, ammonia accumulation in the first part of the catalyst bed decreases. Therefore, total average value of $\theta$ decreases approaches values obtained using the steady-state model (Fig. 4, curve 3).

The essential change of the average adsorbed ammonia content in the catalyst bed as a function of half-cycle time determines purification efficiency. Fig. 5A shows the conversions of $NO_x$ and $NH_3$ calculated using steady- and unsteady-state models. Fig. 5B reflects the maximum temperature obtained with these calculations. Note that at definite half-cycle times (less than 4 min, see Fig. 5A) the reverse process efficiency according to diagram II is higher than the steady state one. Moreover, in steady state ammonia is introduced before the catalyst bed and contact time is twice longer than that in diagram II. The reason is that despite ammonia supply into the catalyst bed center, the adsorbed ammonia distributes over the whole bed length (see Fig. 3A). So, the effective contact time or diagram II coincides with that of diagram I at a constant direction of gas filtering. The dependence calculated via unsteady-state model qualitatively coincides with the experimental results of Ref. [11] (see Fig. 5C). Calculations obtained using the steady-state kinetic model do not allow to describe $NO_x$ conversion dependence of half-cycle time.

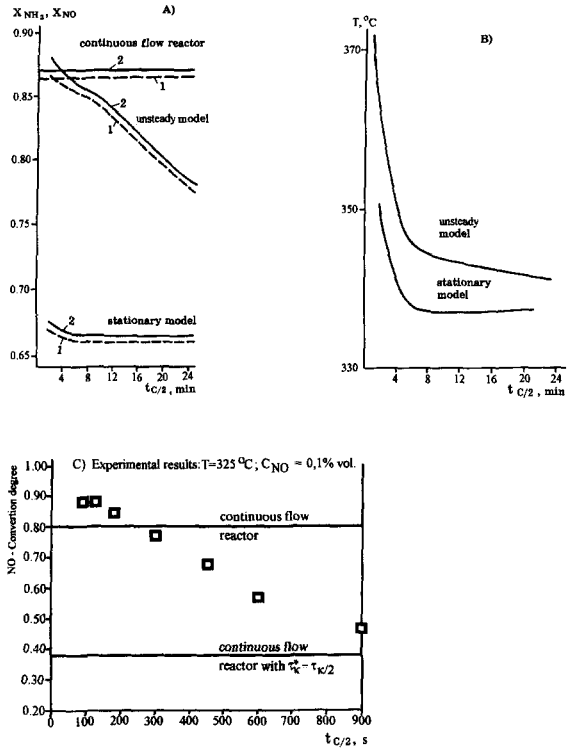


Fig. 5. Nitrogen oxides (curves 1), ammonia (curves 2) conversion (A) and maximum temperature (B) in the catalyst bed versus half-cycle time of reverse-reactor operation (diagram II) (at steady- and unsteady-state models); $C^{in}_{NO_x} = C^{in}_{NH_3} = 0.1$ vol%; (C) – experimental results ([11]).

## 4. Industrial unit for reverse process SCR

For more than six years, an industrial unit purifying gas from nitrogen oxides works at the Biysk oleum plant. It was build according to our design. The process is performed according to diagram II (Fig. 2) with ammonia introduction into the catalyst bed center. In this case the flow sheet of industrial reverse-process SCR looks as shown in Fig. 6.

The plant works in the following manner. At the switched-off supply of nitrous gases ventilator (5) and heater (2) are started. The heating occurs, when switching valves (3) are in the position shown in Fig. 6. The hot air passes inert bed I1 and catalyst bed C1 and through a gas pipe enters the bottom of the reactor. At bottom part of the reactor air passes through catalyst bed C2 and inert bed I2,

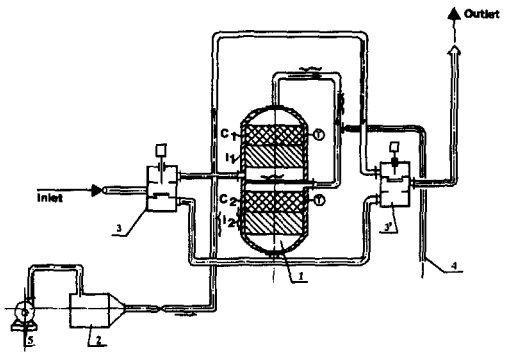


Fig. 6. Flow sheet of industrial plant. 1 – reactor, 2 – starting heater, 3,3′ – valves, 4 – ammonia supply line, 5 – starting ventilator, $T$ – thermal couples for control.

and exhausted into the atmosphere through outlet valve 3.

The heating occurs for 6–8 h until the temperature in catalyst bed C2 attains 220–250°C. Then electric heater and air supplied are switched off, and gases after absorption start to come to the purifying plant. The exhaust gases at a temperature of 30–50°C pass the hot grain material where they are heated. In a connecting gas pipe, ammonia water is introduced through a distributor into the heated reaction mixture. The heat of gases is expended in evaporation and heating of ammonia water up to a temperature which provides a high rate of $NO_x$ reduction by ammonia. Reaction mixture mixed with ammonia water comes to catalyst bed C2, where $NO_x$ react with ammonia thus producing heat. Then hot purified gas pass inert bed 12, where they give their heat to an inert packing and cool. Through outlet valve (3′) the purified gases are exhausted into the atmosphere. Heat transfer to inlet gas from thus cooling inert and catalyst beds I1 and C2 is monitored by thermal couple $T$. As the gas temperature at the inlet to bed C1 decreases to 180–270°C, valves (3,3′) are re-switched and initial reaction mixture appears at the bottom part of the reactor onto the earlier heated inert and catalyst beds I2 and C2. After reaction mixture passes these beds, ammonia water is introduced and then exothermic reduction reaction occurs in catalyst bed C1. The purified hot gases go through inert bed I1 and through outlet valve (3′) into the atmosphere. Ammonia water supply is set depending on the concentration of nitrogen oxides in the exhaust gases. Ammonia water is supplied

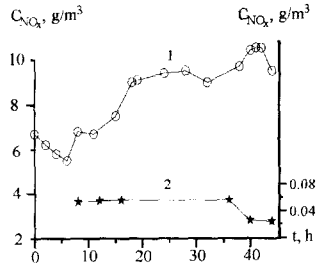


Fig. 7. Concentration of nitrogen oxides at the inlet (1) and outlet (2) of industrial unit.

through the heated pipe and is almost completely evaporated before it comes to the reactor.

In the large scale plant the concentrations of nitrogen oxides at the plant inlet changes during a day by more than twofold (see curve 1, Fig. 7). The control over reductant (ammonia water) supply occurs every 2 h. Accounting for the catalyst bed capacity toward ammonia adsorption such a control is enough for efficient plant work. Fig. 7 shows the control test results during two days. At widely oscillating inlet $NO_x$ concentrations, the outlet ones do not exceed 70 mg/m$^3$ (see curve 2, Fig. 7). No ammonia was registered at the outlet in 90% of tests.

As the concentration decreases, the time period between the switches is automatically reduced thus maintaining the maximum temperature in the catalyst bed at 280–300°C and providing efficient purification. Fig. 8 shows the daily chart of the temperature change

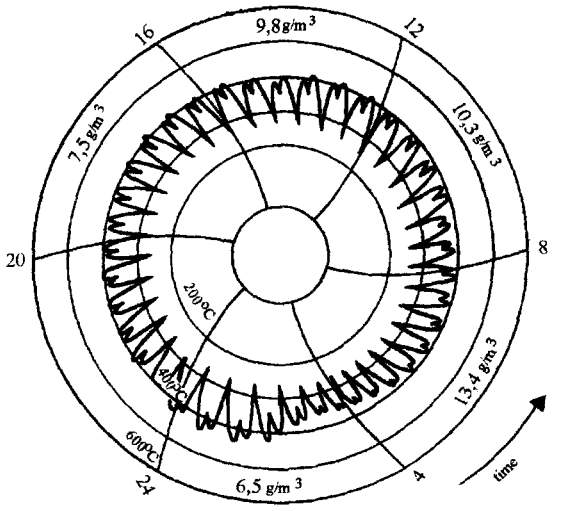


Fig. 8. Daily chart of temperature change on the control thermal couple of industrial plant.

on one of the thermal couples. One can correlate the change of semi-cycle time with $NO_x$ concentration changing in the purified gas. At the beginning $NO_x$ concentration was 6.5 g/m$^3$, and the time decreases progressively from 45 to 27 min. The maximum temperatures fell from 415 to 360°C. The switching occurred as the temperature on the thermal couple decreases to 240°C. The further increase of $NO_x$ concentration to 13.4 g/m$^3$ resulted in increase of the temperature and cycle time. Temperature grew to 400°C, and time to 40 min. Due to the system

Table 1
Parameters of industrial plant purifying gases from nitrogen oxides

| Parameter | Range | Average value |
|---|---|---|
| Volume of gases to be purified, (m$^3$/h) | 9.0–10.8 | 10.0 |
| Catalyst bed length (m) | 2 × 0.55 | 2 × 0.55 |
| Inert bed length (m) | 2 × 0.5 | 2 × 0.5 |
| Inlet $NO_x$ concentration (g/m$^3$) | 2–11 | 5.7 |
| Ammonia water supply (l/h) | 90–220 | 160 |
| Outlet $NO_x$ concentration (g/m$^3$) | 0.02–0.3 | 0.07 |
| Purification degree (%) | 94.0–99.5 | 96.7 |
| Outlet $NH_3$ content (g/m$^3$) | No ammonia in 90% of samples, $C_{max}$ = 0.08 | |
| Inlet gas temperature (°C) | 20–40 | 30 |
| Reactor temperature (°C) | 300–450 | 350 |
| Pressure drop, (mm) | 550–600 | 580 |
| Energy consumed for gas heating | None | None |
| Time between switching (min) | 5–25 | 18 |

inertia, the time between switches changes with some delay (see the concentration decrease from 10.3 to 7.5 g/m$^3$). Note that at first the cycle time shortens and only then the maximum temperature decreases. For example, at 5 p.m. the cycle time was 40 min, but the maximum temperature was still 400°C. Only at 8 p.m. temperature fell to 390–380°C.

Note once again that a large ammonia adsorption capacity of the SCR catalysts is of key importance. It provides considerable ammonia accumulation in the catalyst bed and its consumption as the concentration of $NO_x$ changes. In reverse process this catalyst property is most efficiently used.

Table 1 lists the main plant parameters during its operation since 1989. Note, first of all, almost zero $NH_3$ concentration at the plant outlet due to its adsorption in the catalyst bed.

At an inlet $NO_x$ concentration of 5–10 g/m$^3$ heat evolving in the reaction is sufficient to provide an autothermal regime, while the ammonia adsorption capacity of the catalyst allows to maintain a good purification efficiency at the deviations of $NO_x/NH_3$ stoichiometry.

## 5. Conclusions

The mathematical modeling of SCR processes performed under periodic oscillations of the composition, and/or at the reverse of the filtered gas flows in the catalyst bed, helped to reveal significant effect of the unsteady catalyst surface state on the process efficiency. The periodic changes in temperature and composition of reaction mixture allow to maintain the catalyst activity far above the steady-state level, thus providing the maximum purification degree. In theory, the half-cycle time was found to affect the distribution of adsorbed ammonia over the catalyst bed. In the SCR performance under the periodic gas flow reverse the heat inertia of the catalyst as well as the mass accumulation of ammonia are used.

Reactor mathematical model using the unsteady-state kinetic process model helped to describe qualitatively the high experimental values of $NO_x$ removal and to explain theoretically how less than 50 ppm outlet $NO_x$ concentrations are obtained in the large scale plants.

## 6. Nomenclature

| | |
|---|---|
| $C_i$ | gas concentrations of ammonia ($i = 1$) and nitrogen oxides ($i = 2$), vol%. |
| $\hat{C}_i$ | catalyst concentrations of ammonia ($i = 1$) and nitrogen oxides ($i = 2$), vol%. |
| $C_p$ | heat capacity of gas, kJ m$^{-3}$ K$^{-1}$. |
| $C_c$ | heat capacity of catalyst, kJ m$^{-3}$K$^{-1}$. |
| $S$ | specific external surface of particles per bed volume unit, m$^2$ m$^{-3}$. |
| $U$ | linear reaction mixture velocity (calculated for standard conditions and full bed sequence), m s$^{-1}$. |
| $a$ | catalyst bed adsorption capacity, dimensionless (m$^3$ of gaseous ammonia per 1 m$^3$ catalyst). |
| $l$ | axial coordinate, m. |
| $T$ | temperature, °C. |
| $W_i$ | reaction rates, s$^{-1}$. |
| $Q_i$ | heat effect of reactions $i$, kJ m$^{-3}$. |
| $t$ | physical time of the system, s. |
| $L$ | bed length, m. |
| $k_1^{\pm}$, $k_2$, $k_3$ | rate constants, s$^{-1}$. |
| $t_{c/2}$ | half-cycle duration, min. |

## 7. Greek letters

| | |
|---|---|
| $\alpha_0$ | heat transfer coefficient, m s$^{-1}$. |
| $\beta_0$ | mass transfer coefficient, m s$^{-1}$. |
| $\lambda_{eff}$ | effective coefficient of axial thermal conductivity of catalyst, kJ m$^{-1}$ s$^{-1}$ K$^{-1}$. |
| $\gamma$ | dimensionless relative volume heat capacity of catalyst bed. |
| $\varepsilon$ | void fraction. |
| $\theta$ | fractional surface coverage of adsorbed ammonia. |
| $\Delta T_{ad,i}$ | adiabatic heating in $i$th reaction, K. |
| $\tau_c$ | contact time, s. |

## 8. Indices

| | |
|---|---|
| in | inlet. |
| o | initial. |
| s | solid phase. |
| + | adsorption. |
| − | desorption. |

## References


[1] Yu.Sh. Matros, Catalytic Process Under Unsteady-State Conditions, Elsevier, Amsterdam, 1989.

[2] Matros Yu.Sh., A.S. Noskov, V.A. Chumachenko and O.V. Goldman, Chem. Eng. Sci., 43 (1988) 2061–2068.

[3] U. Nieken, G. Koils and G. Eigenberger, Catal. Today, 20 (1994) 335–350.

[4] Bert van de Beld, K. Roel Westerterp, Chem. Eng. Technol., 17 (1994) 217-226.

[5] G.K. Boreskov and Yu.Sh. Matros, Catal. Rev. Sci. Eng., 25 (1983) 551–590.

[6] L. Lietti and P. Forzatti, J. Catal., 147 (1994) 241.

[7] H. Scheider, S. Tschudin, M. Schneder, A. Wokaun and A. Baiker, J. Catal., 5 (1994) 147.

[8] N. Topsoe, H. Topsoe and J.A. Dumesic, J. Catal., 151 (1995) 226.

[9] N. Topsoe, J.A. Dumesic and H. Topsoe, J. Catal., 151 (1995) 241.

[10] D.W. Agar and W. Ruppel, Chem. Ing. Techn., 60 (1988) 731–741.

[11] K. Heiden, B.R. Rao and N. Schon, Chem. Ing. Techn., 65 (1993) 1506–1508.

[12] A.S. Noskov, L.N. Bobrova and Yu.Sh. Matros, Catal. Today, 17 (1993) 293–300.

[13] Patent USA 5401479.

[14] E. Tronconi, G. Riccardi, P. Forzatti, A. Baldacci, S. Malloggi; G. Centi et al. (Eds.), Environmental Catalysis, SCI Pub: Rome, Italy, (1995) 219.

[15] J.J.P. Biermann, F.J.J.G. Janssen and J.R.H. Ross, J. Phys. Chem., 94 (1990) 8598.

[16] J.B. Lefers, P. Lodder and G.D. Enoch, Chem. Eng. Technol., 14 (1991) 192.

[17] G. Eigenberger, Chem. Eng. Sci., 27 (1972) 1909-1915, 1917-1927.

[18] Yu.Sh. Matros, A.G. Ivanov and L.L. Gogin, Theor. Osnov. Chim. Technol., 22 (1988) 481–487.